Journal of Magnetism and Magnetic Materials 592 (2024) 171808

Contents lists available at ScienceDirect

Journal of Magnetism and Magnetic Materials

journal homepage: www.elsevier.com/locate/jmmm

Research article

Investigation of MHD oxytactic microorganisms with NEPCMs in rectotrapezoidal enclosure with FEM: Applications to energy storage technologies

Shafqat Hussain [a,*], Prakash Jayavel [b], Bander Almutairi [c], Katta Ramesh [d,e,f]

[a] Institut für Angewandte Mathematik (LS III), Fakultät für Mathematik, Technische Universität Dortmund, Germany
[b] Department of Mathematics, Avvaiyar Government College for Women, Karaikal 609 602, U.T of Puducherry, India
[c] Department of Mathematics, College of Science, King Saud University, P.O. Box 2455, Riyadh, 11451, Saudi Arabia
[d] Department of Pure and Applied Mathematics, School of Mathematical Sciences, Sunway University, No. 5, Jalan Universiti, Bandar Sunway, Petaling Jaya 47500, Selangor Darul Ehsan, Malaysia
[e] Department of Mathematics, Graphic Era (Deemed to be University), Dehardun, Uttarakhand, India
[f] Symbiosis Institute of Technology, Symbiosis International (Deemed University), Pune 412115, India

ARTICLE INFO

Keywords:
Nanoparticle-enhanced phase change materials
Higher order GFEM
Rectotrapezoidal cavity
Inclined magnetic field
Oxytactic bacteria

ABSTRACT

Nanoparticle-enhanced phase change materials (NEPCMs) have gained significant attention in recent years due to their unique ability to enhance the thermal properties and overall performance of phase change materials (PCMs). The present work investigates the bioconvection flow of nano-encapsulated phase change material within a rectotrapezoidal cavity. The left wall of the is fixed at the constant high temperature whereas the right vertical wall is kept at cold temperature. The higher order Galerkin finite element method (GFEM) has been employed to simulate the proposed problem. The discrete systems of nonlinear equations are linearized by implementing the adaptive Newtons method. Influence of various pertinent parameters such as inclined magnetic field, oxytactic bacteria, radiation and Lewis number has been analyzed. It is observed that the average Sherwood and Nusselt number exhibit a positive correlation with the Hartmann and radiation parameter. Moreover, the average heat transfer exhibits a decreasing trend as the Hartmann, bioconvection Rayleigh and Peclet increase.

1. Introduction

Nanoparticle-enhanced phase change materials (NEPCMs) have emerged as a promising and innovative class of materials with a wide range of applications across diverse fields. These materials combine the advantageous properties of both nanoparticles and phase change materials (PCMs), resulting in enhanced thermal performance, improved energy efficiency, and novel functionalities. NEPCMs have garnered significant interest from researchers and industries alike due to their potential to address critical challenges in various applications, ranging from energy storage and thermal management to electronics cooling and beyond. Phase change materials are substances that undergo a reversible phase transition, typically from solid to liquid and vice versa, while absorbing or releasing latent heat. This unique behavior allows PCMs to store and release thermal energy over a narrow temperature range, making them ideal candidates for applications requiring efficient heat storage and transfer. However, the practical utilization of PCMs has often been limited by factors such as their relatively low thermal conductivity, cycling stability and phase change temperature range. In recent years, the integration of nanoparticles into phase change materials has emerged as an ingenious strategy to overcome these limitations. Nanoparticles, with their high surface area-to-volume ratios and tunable properties, can significantly enhance the thermal conductivity, heat capacity and cycling stability of PCMs. By judiciously selecting and incorporating nanoparticles into PCMs, researchers have unlocked a multitude of possibilities for NEPCMs in various technological domains. Khodadadi and Hosseinizadeh [1] have concluded from their study that, the NEPCMs demonstrate improved heat conduction when compared to the original material. Shaikh et al. [2] have discussed the latent heat storage capacity was assessed for a system comprising phase change materials (PCMs) infused with carbon nanoparticles and concluded that the model's projected latent energy values exhibited a strong concurrence with the experimental findings. In the study of El Hasadi and Khodadadi [3], the impact of nanoparticle mass transfer on

* Corresponding author.
E-mail address: shafqat.hussain@math.tu-dortmund.de (S. Hussain).

https://doi.org/10.1016/j.jmmm.2024.171808
Received 27 November 2023; Received in revised form 27 January 2024; Accepted 28 January 2024
Available online 30 January 2024

Nomenclature

C_p	specific heat (J kg^{-1} K^{-1})
C	oxygen concentration
D_c	oxygen diffusivity (m^2 s^{-1})
D_n	microorganisms diffusivity (m^2 s^{-1})
E	activation energy parameter
g	gravitational acceleration (m s^{-2})
H	cavity dimension (m)
Ha	Hartmann number
h_{sf}	latent heat of the core (K J kg^{-1})
k	thermal conductivity (W m^{-1} K^{-1})
Le	Lewis number
m	motile microorganisms (dimensional)
m_0	the reference density number
N	motile microorganisms density
Nn	density of the motile microorganisms number
Nu_{avg}	Nusselt number (average)
Pr	Prandtl number
p	pressure (N m^{-2})
Pe	Peclet number
q_r	radiative heat flux
Ra	Rayleigh number
Rd	radiation parameter
Rb	bioconvection Rayleigh number
Sh	Sherwood number
Sc	Schmit number
Sh_{avg}	Sherwood number (average)
Ste	Stefan number
T	temperature (K)
T_{Mr}	melting temperature range
u, v	velocities (m s^{-1})
X, Y	dimensionless Cartesian coordinates
x, y	Cartesian coordinates (m)

Greek symbols

α	thermal-diffusivity (m^2 s^{-1})
β	thermal expansion coefficient (K^{-1})
η	mass ratio of core to the shell
θ	dimensionless temperature
μ	dynamic-viscosity (kg m^{-1} s^{-1})
ν	kinematic-viscosity (m^2 s^{-1})
ξ	oxygen concentration
ρ	density (kg m^{-3})
ϕ	nanoparticles concentration
ψ	stream function

Subscripts

avg	average
b	bulk properties of the suspension
co	properties of the core of NEPCM particle
c	cold
f	water properties
h	hot
p	nanoparticle containing PCM
sh	properties of the shell of NEPCM particle

the solid–liquid interface morphology and changing concentration during the solidification process has been documented. Murugan et al. [4] have explored the melting and solidification behaviors of NPCM. The formulation of NPCM involved the use of paraffin as the phase change material and high-conductivity MWCNT as the nanoparticle, without the use of any dispersant. Irwan et al. [5] have provided a comprehensive review of numerical simulations conducted to investigate the solidification and melting processes of NEPCMs. Li et al. [6] have showcased the findings of a study involving a novel composite phase change material (NCPCM) comprised of nanoparticles, paraffin, and ceramic, designed for applications in latent heat thermal energy storage. Prado and Lugo [7] have provided the formulation of innovative NEPCMs through the dispersion of either graphene nanoplatelets (GnPs) or MgO nanoparticles within a stearate phase change material (PCM). Tariq et al. [8] have provided an extensive review of the methods used to prepare NEPCMs and their diverse applications across various domains such as thermal energy storage (TES), solar thermal energy storage (solar TES), building technologies, electronic cooling, textiles, solar collectors, heat exchangers, photovoltaics (PV), and medical and food packaging. Faraji et al. [9] have examined the positioning of electronic components and the tilt angle of the heat sink, specifically for rectangular and square geometries, collectively influence heat transfer and the flow patterns within a liquid NEPCMs. Within the investigation of Jafarian et al. [10], paraffin wax was infused with aluminum oxide and copper nanoparticles, serving to augment its thermophysical characteristics. In Amidu et al. [11], a numerical model is formulated and applied, integrating an advanced two-phase model for nanoparticles-enhanced phase change materials with the enthalpy-porosity approach to capture the transient phase change behavior.

Complex-shaped enclosures, ranging from irregularly structured environments to intricately designed microfluidic channels, represent a challenging yet pivotal arena for engineering and scientific exploration. The integration of NEPCMs within these complex geometries introduces an unprecedented level of dynamic control over heat transfer mechanisms. Moreover, the study of NEPCMs in complex-shaped enclosures presents a fertile ground for fundamental scientific inquiry. Due to the importance of study of NEPCMs in various complex-shaped structures, many researchers have started their investigation in this direction. Darzi et al. [12] presented a study that aims to employ an enthalpy-based lattice Boltzmann method incorporating a multi-distribution function model to examine the melting process within a cavity containing an obstacle, with natural convection. Elbahjaoui et al. [13] have proposed a numerical exploration of the melting process within a latent heat storage unit (LHSU) using a phase change material (PCM) consisting of Paraffin wax P116 infused with nanoparticles (Al_2O_3). Elbahjaoui and El Qarnia [14] have explored the laminar pulsations in the heat transfer fluid (HTF) impact the melting process of nanoparticle-enhanced phase change material within a shell-and-tube latent heat storage unit (LHSU). Ghalambaz et al. [15] have investigated the melting behavior of phase-change materials enriched with nanoparticles within a square cavity, employing the finite element method. In the study of Masoumi and Khoshkhoo [16], the nanoparticles were dispersed within the phase change material (PCM), and longitudinal fins were simultaneously incorporated into the inner tube to accelerate the melting rate of the PCM in a horizontal shell-and-tube heat exchanger. Ghalambaz et al. [17] have assessed the benefits of employing wavy tubes in unobstructed flows, where convective heat transfer phenomena play a significant role. Abderrahmane et al. [18] have conducted a simulation of natural convection flow within an inverse T-shaped enclosure, utilizing NEPCMs. Hussain et al. [19] have discussed the analysis of bioconvection in an omega-shaped porous enclosure involving oxytactic microorganisms and nano-encapsulated phase change materials. Hussain et al. [20] have presented two-dimensional simulations to analyze the bioconvection flow within a closed porous space containing a quadrant heater and saturated with nano-enhanced phase change material. Qahiti et al. [21] have provided the analysis of the thermal behavior of nanoparticle-enhanced phase change material during discharge in the presence of intricate geometrical configurations. Abdi et al. [22] have examined

two-dimensional, steady-state, laminar flow and natural convection heat transfer within an inclined square enclosure.

The integration of magnetohydrodynamics (MHD), NEPCMs, and cavity fluid flow presents a promising synergy for advanced thermal management applications. MHD principles can be leveraged to control and enhance the fluid flow within enclosed cavities, optimizing heat transfer processes. By incorporating nano-PCMs into the cavity, the phase change material's thermal properties are significantly improved, allowing for efficient absorption and release of thermal energy during phase transitions. This combined approach enables precise control over temperature changes and enhances the overall thermal performance of systems. Potential applications include advanced cooling systems for electronic devices, energy storage with improved efficiency, and thermal management in aerospace applications, where precise control over temperature gradients is crucial for optimal performance and reliability. Rahmani et al. [23] conducted a study on the melting process of phase change material (PCM) in a battery pack, specifically investigating the impact of the MHD effect on PCM melting. Aly et al. [24] focused on optimizing energy efficiency by controlling heat transfer and fluid flow through the use of differently shaped materials under various forces and boundary conditions. Specifically, they investigated the impact of thermal radiation on MHD thermosolutal convection of NEPCMs suspension within a horizontal wavy porous cavity featuring embedded high-temperature crescents. Younis et al. [25] investigated magnetohydrodynamic mixed convection of NEPCMs within a lid-driven trapezoidal prism enclosure containing a hot-centered elliptical obstacle. Zandie et al. [26] analyzed a 2D cubic chamber model filled with paraffin, examining the effects of adding magnetic iron oxide nanoparticles at different concentrations (0.5, 1, 1.5, and 2 wt%) and subjecting the system to external magnetic fields with intensities ranging from 0.005 to 0.02 T.

Oxytactic microorganisms and nanoparticle-enhanced phase change materials represent two distinct yet interconnected realms of scientific inquiry that hold great promise for advancing various fields, including environmental remediation, bioengineering, and materials science. Oxytactic microorganisms, characterized by their ability to exhibit directed movement in response to oxygen gradients, have captivated researchers for their potential applications in bioremediation, biofuel production, and sensing technologies. The research (oxytactic microorganisms and nanoparticle-enhanced phase change materials) endeavors to investigate the potential applications and benefits of utilizing oxytactic microorganisms to actively manipulate the thermal behavior of NEPCMs, thereby paving the way for groundbreaking advancements in various domains. Oxytactic microorganisms possess an innate ability to migrate towards oxygen-rich environments, a phenomenon that has inspired innovative strategies in environmental remediation. Integrating these microorganisms with NEPCMs introduces a dynamic element, wherein the microorganisms' oxygen-seeking behavior can be harnessed to induce localized phase transitions within the NEPCMs. Such interactions open avenues for responsive thermal regulation, self-healing materials, and controlled heat release mechanisms that could find applications in self-sustaining temperature management systems and next-generation thermal energy storage technologies. To the best of the authors' knowledge, the combination of oxytactic microorganisms and nanoparticle-enhanced phase change materials within intricate enclosures has not been previously explored in the literature. Given this context, the present study is dedicated to investigating the bioconvection flow of NEPCMs within a rectotrapezoidal cavity. The investigation employs the finite element method and considers the influence of an inclined magnetic field, oxytactic bacteria, and radiation.

2. Model of the problem

Fig. 1 depicts the initial diagram of a physical model, which consists of a rectotrapezoidal shaped cavity of side length H. The cavity is saturated with a water based suspension of nano-encapsulated phase

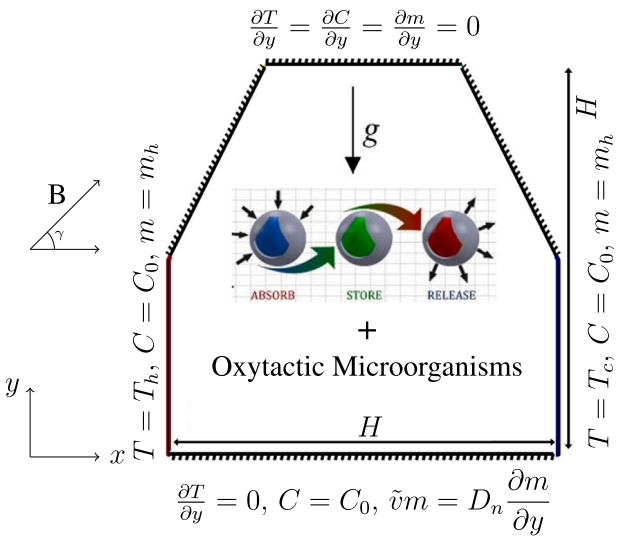

Fig. 1. The problem configuration.

Table 1
Thermal characteristics of NEPCM suspension [27,28].

	Material	ρ	$\beta \times 10^{-5}$	C_p	k
Host fluid	Water	997.1	21	4179	0.613
Core	Nonadecane	786	17.28	1317.7	–
Shell	Polyurethane	721	–	2037	–
Porous matrix	Glass balls	2700	–	840	1.05

change materials in the presence of oxytactic microorganisms. The phase change nanoparticles are assumed to be well dispersed in the base fluid. All the walls of the cavity are subjected to the no-slip velocity boundary condition. The left vertical wall of the cavity is maintained at the constant high temperature whereas the right vertical wall is kept at cold temperature. All the remaining walls are kept insulated. Under the prescribed boundary conditions, the proposed problem is assumed to be natural convective, laminar, steady, incompressible, and bioconvection flow. The nano-encapsulated phase-change materials consists of the core and shell as the encapsulation material, see [27–29] for further details. The core of NEPCM undergoes a phase transition at the fusion temperature (T_f). During the phase transition to liquid, it absorbs/releases its energy in the form of latent heat. The proposed configuration is further subjected to the following assumptions:

- The suspension of nanoparticles is uniform and stable.
- The local thermal equilibrium is applied amongst a base fluid and NEPCMs.
- Adding nanoparticles is not affecting on the velocity and direction of bacteria's swimming.
- The magnetic field is imposed to be an inclined with a strength B_0.
- The effect of activation energy and thermal radiations are also taken into consideration.
- Induced magnetic field, Joule heating and viscous dissipation effects are neglected.
- The temperature variations are small and Boussinesq approximation is applied for the density changes.

2.1. The thermophysical features of the suspension

The thermophysical properties of the nanoparticles and the base fluid are demonstrated in Table 1

The Thermophysical properties of the bulk suspension involved in the controlling partial differential equations (PDEs) need to be

evaluated before solving the obtained model, in which the related characteristics of water and NEPCMs are denoted by the subscripts f and p, respectively, [27,28]. The density of the suspension can be computed as

$$\rho_b = (1-\phi)\rho_f + \phi\rho_p, \tag{1}$$

in which the density of NEPCMs particles (ρ_p) is calculated as

$$\rho_p = \frac{(1+\eta)\rho_{co}\rho_{sh}}{\rho_{sh}+\eta\rho_{co}}. \tag{2}$$

Here, η is the mass ratio of the core to shell and is approximated as $\eta = 0.447$. The heat capacity of the bulk suspension $(C_{p,b})$ is evaluated as

$$C_{p,b} = \frac{(1-\phi)\rho_f C_{p,f} + \phi\rho_p C_{p,p}\big|_{eff}}{\rho_b} \tag{3}$$

where $C_{p,p}\big|_{eff}$ is the effective specific heat of NEPCMs particles and computed as follows in the absence of phase change

$$C_{p,p}\big|_{eff} = \frac{\left(C_{p,co}+\eta C_{p,sh}\right)\rho_{co}\rho_{sh}}{\left(\rho_{sh}+\eta\rho_{co}\right)\rho_b}. \tag{4}$$

By taking into account the phase change transition, there is an increase in specific heat capacity which can be achieved through the sinusoidal profile [27]

$$C_{p,p}\big|_{eff} = C_{p,b} + \left\{\frac{\pi}{2}\cdot\left(\frac{h_{sh}}{T_{Mr}} - C_{p,p}\right)\cdot\sin\left(\pi\frac{T-T_0}{T_{Mr}}\right)\right\}\cdot \begin{cases} 0 & \text{if } T < T_0 \\ 1 & \text{if } T_0 < T < T_1 \\ 0 & \text{if } T > T_1 \end{cases} \tag{5}$$

The factor $\frac{\pi}{2}C_{p,b}$ can be ignored as $C_{p,b}$ is very small in comparison with $\frac{h_{sh}}{T_{Mr}}$. T_0 and T_1 denote the down and top margins of the melting temperature, T_{Mr}, expressed as [27]

$$T_0 = T_{fu} - \frac{T_{Mr}}{2}, \qquad T_1 = T_{fu} + \frac{T_{Mr}}{2}. \tag{6}$$

where T_{fu} is a fusion temperature. For a suspension, the thermal volume expansion is:

$$\beta_b = \phi\beta_p + (1-\phi)\beta_f. \tag{7}$$

The following linear relationships are employed for viscosity and thermal conductivity of the suspension:

$$\frac{\mu_b}{\mu_f} = 1+\chi_1\phi, \qquad \frac{k_b}{k_f} = 1+\chi_2\phi, \qquad \frac{\sigma_b}{\sigma_f} = 1+\chi_3\phi. \tag{8}$$

The constants, χ_1, χ_2 and χ_3 representing the corresponding numbers of dynamic viscosity, thermal conductivity and electrical conductivity are given as $\chi_1 = 12.5$, $\chi_2 = 23.8$, and $\chi_3 = 3$.

2.2. The governing equations

The proposed problem can be modeled using the conservation laws of mass, momentum, energy, oxygen and microorganism conservation as follows [27–29]:

$$\frac{\partial u}{\partial x} + \frac{\partial v}{\partial y} = 0 \tag{9a}$$

$$\mu_b\nabla^2 u = \frac{\partial p}{\partial x} + \rho_b\left(u\frac{\partial u}{\partial x} + v\frac{\partial u}{\partial y}\right) + f_u \tag{9b}$$

$$\mu_b\nabla^2 v = \frac{\partial p}{\partial y} + \rho_b\left(u\frac{\partial v}{\partial x} + v\frac{\partial v}{\partial y}\right) + f_v \tag{9c}$$

$$\alpha_b\nabla^2 T = u\frac{\partial T}{\partial x} + v\frac{\partial T}{\partial y} + \frac{\partial q_r}{\partial y} \tag{9d}$$

$$D_c\nabla^2 C = u\frac{\partial C}{\partial x} + v\frac{\partial C}{\partial y} + \delta m + k_r^2(C-C_{min})\left(\frac{T}{T_c}\right)^n \exp(-E_a/GT) \tag{9e}$$

$$\frac{\partial}{\partial x}\left[um + \tilde{u}m - D_n\frac{\partial m}{\partial x}\right] + \frac{\partial}{\partial y}\left[vm + \tilde{v}m - D_n\frac{\partial m}{\partial y}\right] = 0, \tag{9f}$$

where the body forces are given as

$$f_u = \sigma_b B_0^2\left(v\sin\gamma\cos\gamma - u\sin^2\gamma\right) \tag{10a}$$

$$f_v = \sigma_b B_0^2\left(u\sin\gamma\cos\gamma - v\cos^2\gamma\right) + (\gamma^\star\Delta\rho\cdot m - (\rho\beta)_b(T-T_c))g. \tag{10b}$$

The symbols $\tilde{u} = \left(\frac{bW_c}{\Delta C}\right)\frac{\partial C}{\partial x}$ and $\tilde{v} = \left(\frac{bW_c}{\Delta C}\right)\frac{\partial C}{\partial y}$ explain the mean swimming velocities of bacteria. C_0 represents the oxygen concentration for right and left walls, W_c is the maximum cell swimming speed, δm denotes the oxygen usage of bacteria, $\gamma^\star$ representing the mean volume of bacteria and $\Delta C = C_0 - C_{\min}$ where $C_{\min}$ is a minimum oxygen concentration. The radiative heat flux is adopted by Rosseland approximation [30] as $q_r = -(4\sigma_B/3\beta_R)(\partial T^4/\partial y)$, where σ_B and β_R are the Stefan-Boltzmann constant and the mean absorption coefficient, respectively. Under the assumption of small temperature differences, the temperature T^4 is approximated about T_c using the well-known Taylor series expansion

$$T^4 \approx 4T_c^3 T - 3T_c^4 \tag{11}$$

and

$$\frac{\partial q_r}{\partial y} = -\left(\frac{16\sigma_B T_c^3}{3\beta_R}\right)\frac{\partial^2 T}{\partial y^2}. \tag{12}$$

The dimensional system (9) is reduced to the dimensionless form with the following transformations

$$X = \frac{x}{H}, Y = \frac{y}{H}, U = \frac{uH}{\alpha_f}, V = \frac{vH}{\alpha_f}, P = \frac{pH^2}{\rho_f\alpha_f^2}, \tag{13a}$$

$$\theta = \frac{T-T_c}{T_h-T_c}, \xi = \frac{C-C_{\min}}{\Delta C}, N = \frac{m}{m_h}, \alpha_f = \frac{k_f}{(\rho C_P)_f} \tag{13b}$$

The following dimensionless form of PDEs is achieved with the help of above variables [27–29]:

$$\frac{\partial U}{\partial X} = -\frac{\partial V}{\partial Y}, \tag{14a}$$

$$Pr(1+N_v\phi)\nabla^2 U = \frac{\partial P}{\partial X} + \left(\frac{\rho_b}{\rho_f}\right)\left(U\frac{\partial U}{\partial X} + V\frac{\partial U}{\partial Y}\right) + F_U \tag{14b}$$

$$Pr(1+N_v\phi)\nabla^2 V = \frac{\partial P}{\partial Y} + \left(\frac{\rho_b}{\rho_f}\right)\left(U\frac{\partial V}{\partial X} + V\frac{\partial V}{\partial Y}\right) + F_V \tag{14c}$$

$$\frac{k_b}{k_f}\left[\frac{\partial^2\theta}{\partial X^2} + \left(1+\frac{4Rd}{3}\right)\frac{\partial^2\theta}{\partial Y^2}\right] = Cr\left(U\frac{\partial\theta}{\partial X} + V\frac{\partial\theta}{\partial Y}\right) \tag{14d}$$

$$\frac{1}{Le}\nabla^2\xi = U\frac{\partial\xi}{\partial X} + V\frac{\partial\xi}{\partial Y} + \frac{\zeta}{Le}N + \frac{RcSc}{Le}\xi(1+\epsilon_1\theta)^n\exp(-E/(1+\epsilon_1\theta)) \tag{14e}$$

$$\frac{1}{Le}\nabla^2 N = \chi\left(U\frac{\partial N}{\partial X} + V\frac{\partial N}{\partial Y}\right) + \frac{Pe}{Le}\left(N\frac{\partial^2\xi}{\partial X^2} + N\frac{\partial^2\xi}{\partial Y^2} + \frac{\partial N}{\partial X}\frac{\partial\xi}{\partial X} + \frac{\partial N}{\partial Y}\frac{\partial\xi}{\partial Y}\right), \tag{14f}$$

where

$$F_U = \left(\frac{\sigma_b}{\sigma_f}\right)\left(\frac{\rho_f}{\rho_b}\right)\left(V\sin\gamma\cos\gamma - U\sin^2\gamma\right) \tag{15a}$$

$$F_V = \left(\frac{\sigma_b}{\sigma_f}\right)\left(\frac{\rho_f}{\rho_b}\right)\left(U\sin\gamma\cos\gamma - V\cos^2\gamma\right) - RaPr\left(\frac{\rho_b}{\rho_f}\right)\left(\frac{\beta_b}{\beta_f}\right)(\theta - R_bN) \tag{15b}$$

where $\chi = D_c/D_n$ depicts the diffusion ratio and $\zeta = (m_0\delta H^2/(D_c\Delta C))$ denotes the consumption of oxygen. The heat capacity ratio Cr in Eq. (14d) is given by

$$Cr = (\rho C_p)_b/(\rho C_p)_f = (1-\phi) + \phi\lambda + \frac{\phi}{\delta Ste}f. \tag{16}$$

The involved parameters in (14) such as Prandtl, Rayleigh, bioconvection Rayleigh, Hartmann, Peclet, Lewis, activation energy, reaction

rate, Schmidt number and temperature difference are given by:

$$Pr = \frac{\nu_f}{\alpha_f},\ Ra = \frac{\beta_T g H^3 \Delta T Pr}{\nu^2},\ Rb = \frac{m_0(\rho_{cell} - \rho_f)\gamma}{\rho_f \beta_f (T_h - T_c)}, \tag{17a}$$

$$Ha = B_0 H \sqrt{\frac{\sigma_f}{\mu_f}},\ Pe = \frac{bW_c}{D_n},\ Le = \frac{\alpha_f}{D_c},\ E = \frac{E_a}{GT_c}, \tag{17b}$$

$$Rc = \frac{k_r^2 H^2}{\nu_f},\ Sc = \frac{\nu_f}{D_c},\ \epsilon_1 = \frac{T_h - T_c}{T_c},\ Rd = \frac{4\sigma_B T_c^3}{k_f \beta_R} \tag{17c}$$

The ratio of the sensible-heat capacity of NEPCMs particles to the base fluid (λ), the dimensionless melting temperature range (δ) and the Stefan number (Ste) are defined as [27]:

$$\lambda = \frac{\left(C_{p,co} + \eta C_{p,sh}\right)\rho_{co}\rho_{sh}}{\left(\rho C_p\right)_f \left(\rho_{sh} + \eta \rho_{co}\right)},\qquad \delta = \frac{T_{Mr}}{\Delta T},\qquad Ste = \frac{\Delta T \left(\rho C_p\right)_f \left(\rho_{sh} + \eta \rho_{co}\right)}{h_{sf}\rho_{co}\rho_{sh}(1+\eta)}. \tag{18}$$

The fusion function (f) can be written as a function of dimensionless temperature

$$f = \left\{\frac{\pi}{2} \cdot \sin\left(\frac{\pi}{\delta}\left(\theta - \theta_f + \frac{\pi}{2}\right)\right)\right\} \cdot \begin{cases} 0 & \text{if} \quad \theta < \theta_f - \frac{\delta}{2} \\ 1 & \text{if} \quad \theta_f - \frac{\delta}{2} < \theta < \theta_f + \frac{\delta}{2} \\ 0 & \text{if} \quad \theta > \theta_f + \frac{\delta}{2} \end{cases} \tag{19}$$

Here the fusion temperature $\left(\theta_f\right)$ may be expressed as

$$\theta_f = \frac{T_f - T_c}{T_h - T_c}. \tag{20}$$

2.3. The dimensionless boundary conditions

The no-slip velocity $U = V = 0$ are prescribed for all the cavity boundaries. Thermal and concentration components are subjected to the following constraints

On the left vertical wall: $\xi = N = 1, \theta = 1$

On the right vertical wall: $\xi = N = 1, \theta = 0$

On the bottom wall: $\frac{\partial \theta}{\partial Y} = 0,\ \xi = 1,\ PeN\frac{\partial \xi}{\partial Y} = \frac{\partial N}{\partial Y}$

On the other walls: $\frac{\partial \theta}{\partial Y} = \frac{\partial \xi}{\partial Y} = \frac{\partial N}{\partial Y} = 0.$

2.4. The stream function (ψ)

The stream function can be used in order to plot and analyze the streamlines of the flow field. For the two-dimensional flow, the velocity components and the stream function are related as

$$U = -\frac{\partial \psi}{\partial Y},\quad V = \frac{\partial \psi}{\partial X}. \tag{21}$$

2.5. The Nusselt number (Nu), Sherwood number of oxygen (Sh) and density of motile microorganisms (Nn)

The corresponding quantities of interest, namely, local and average Nusselt number, Sherwood number of oxygen and density of motile microorganisms. These quantities at the local level are defined as

$$Nu_{\text{loc}} = -\frac{k_b}{k_f}\frac{\partial \theta}{\partial X},\quad Sh_{\text{loc}} = -\frac{\partial \xi}{\partial X},\quad Nn_{\text{loc}} = -\frac{\partial N}{\partial X}. \tag{22}$$

For the corresponding average quantities, each of the above is integrated over the heated section

$$Nu_{\text{avg}} = \int_0^S Nu_{\text{loc}} dS,\quad Sh_{\text{avg}} = \int_0^S Sh_{\text{loc}} dS,\quad Nn_{\text{avg}} = \int_0^S Sh_{\text{loc}} dS, \tag{23}$$

where S is the length of the heated portion.

Table 2
Comparison for the average Nu between the present study and Ref. [34] for $\phi = 0.04$.

Ha	Nu_{avg}		$\lvert\psi\rvert_{\max}$	
	Present	Ref. [34]	Present	Ref. [34]
0	4.899	4.896	11.589	11.561
15	4.217	2.211	8.759	8.734
30	3.131	3.124	5.668	5.642
45	2.324	2.317	3.652	3.629
60	1.821	1.815	2.433	2.415

Table 3
The grid sensitivity analysis.

ℓ	#EL	Nu_{avg}	Sh_{avg}	Nn_{avg}
1	186	7.87060	0.60035	0.42177
2	322	8.07888	0.61314	0.43396
3	503	8.30065	0.61802	0.43634
4	896	8.46359	0.62503	0.43949
5	1356	8.57452	0.62844	0.43889
6	2214	8.64343	0.63197	0.43998
7	5904	8.87773	0.64130	0.44117
8	15 245	9.03287	0.64656	0.44142
9	23 301	9.03041	0.64660	0.44167

3. Numerical procedure

The dimensionless form (14) of a physical problem is simulated by using the Galerkin based finite element method (FEM). The computational domain is discretized using quadratic ($\mathbb{P}_2$) elements for the U, V, θ, ξ, N and linear ($\mathbb{P}_1$) finite elements for the approximation of pressure. The discrete system of nonlinear equations has been handled with the help of adaptive Newtons method. The linear system of equations in each nonlinear sweep, has been solved using the Gaussian elimination method. The nonlinear outer loop is terminated when the nonlinear residual drops down by 10^{-6} and the last iteration is accepted as the approximate solution. The solution procedure has already been employed and explained in our earlier work, see for example, [31,32] for details.

3.1. The validation tests

The adopted solver has been validated in [33] against the numerical and experimental studies. To check the authenticity of the designed solver for the magnetohydrodynamics natural convection flow of nanofluid, it is also validated for the reference study [34] for various values of Hartmann number. A very close agreement between the results is demonstrated in Table 2.

3.2. The grid independence study

The grid independence test is performed for the average Nu, Sh and Nn for $Pe = 1, Ste = \theta_f = 0.5, \chi = \zeta = 1, Pr = 6.2, \phi = 0.05, Ha = 25, \gamma = 0, Ra = 10^5, Rd = 1, Rc = 0.5, Sc = 1, E = 0.5, n = 0.5$ and $Rb = 10$. The total number of elements (EL) at each level ℓ and the corresponding obtained results are demonstrated in Table 3 which shows insignificant variations in the chosen quantities for the highest computed level $\ell = 8$ (see Fig. 2). So, $\ell = 8$ is found appropriate for the numerical simulation.

4. Numerical results

The numerical findings of this work demonstrate the influence of a sloped Lorentz force on the motion of a Newtonian nanoliquid in a cavity with complex geometric features. The cavity is filled with NEPCMs and oxytactic microorganisms. The combination of nano-enhanced phase change materials with oxytactic microorganisms forms a highly efficient system capable of efficiently storing and releasing

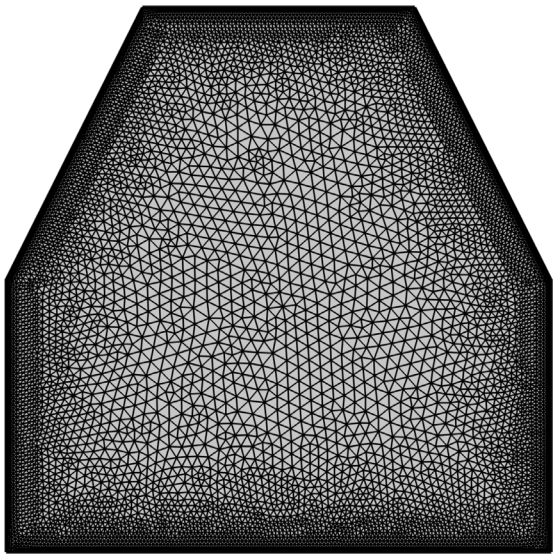

Fig. 2. The designed grid at level $\ell = 8$.

thermal energy. The NEPCMs function as reservoirs, whilst the microbes serve as the distribution mechanism. This combination has versatile potential for a range of applications, including but not limited to temperature regulation in buildings, enhancement of solar panel efficiency, and the development of self-heating apparel. This section focuses on the influence of various fluid parameters, including the Hartmann number ($Ha = 25 - 100$), Rayleigh number ($Ra = 10^3 - 10^7$), thermal radiation ($Rd = 0 - 4$), and Lewis number ($Le = 0.1 - 10$), on several quantities such as streamlines (ψ), isotherms (θ), oxygen concentration (ξ), motile microorganisms (N), heat capacity ratio (Cr), Nusselt number (Nu), oxygen sherwood number (Sh), and density of motile microorganisms (Nn) within a cavity that possesses intricate geometric characteristics (refer to Fig. 1). The parameters have been assigned the following standard values unless otherwise mentioned: $Pe = 1, Ste = \theta_f = 0.5, \chi = \zeta = 1, Pr = 6.2, \phi = 0.05, Ha = 25, \gamma = 0, Ra = 10^5, Rd = 1, Rc = 0.5, Sc = 1, E = 0.5, n = 0.5$ and $Rb = 10$. Additionally, the Pr is held constant at a value of 6.2, signifying the utilization of water at a temperature of 25^0C.

4.1. Impact of Hartmann number (Ha)

The investigation focuses on the analysis of the impact of the manipulated magnetic field by altering the Hartmann number within the range of 25 to 100, while maintaining a constant Prandtl number of 6.2. Fig. 3 has been constructed in order to observe the impact of the Ha on various profiles, including ψ, θ, ξ, N, Cr. In the context of the streamline pattern, the Hartmann number affects the flow patterns of the electrically conductive fluid within the enclosure. At a magnetic field strength of $Ha = 25$, the presence of clockwise recirculating eddies over the obstacle within both the top and bottom edges of the enclosure has been observed. The majority of the streamlines exhibit a pronounced concentration in close proximity to the lower flexible surface, suggesting a heightened fluid velocity in this particular region. Conversely, a sparser distribution of streamlines has been noted at a greater distance from the top flexible surface. As the magnetic field approaches $Ha = 50$, there is a decrease in the circulation of flow, indicating a reduction in the fluid flow. Additionally, a concentration of streamlines is observed in close proximity to the upper movable wall. When the value of Ha is set to 100, it can be observed that the streamlines are confined to a localized region resembling a plume over the complex-shaped enclosure. This confinement occurs due to the influence of a magnetic field, which generates a Lorentz force opposing the direction of fluid flow. As a result, there is a decrease in the fluid flow entering the cavity. The presence of a magnetic field induces curvature and torsion in the isotherms. An increased Hartmann number corresponds to an intensified magnetic field, resulting in augmented heat transfer as a consequence of the magnetic drag exerted on the fluid. Consequently, this phenomenon has an impact on the distribution of temperature and leads to modifications in the patterns of isotherms. The presence of a magnetic field can impede fluid motion, leading to a decrease in heat transfer within specific regions. The impact of the Hartmann number on concentration patterns is contingent upon the particular problem at hand and the characteristics of the substances being transported. When the distribution of some species is affected by the flow of fluids and changes in temperature, such as in natural convection or diffusion-driven processes, the Hartmann number can indirectly affect the patterns of concentration by changing the flow patterns and temperature distribution. Applying a magnetic field may cause the solute to gather in certain areas of the fluid flow. The Hartmann number has an impact on the diffusion rate of the solute, with higher Hartmann numbers resulting in decreased diffusion rates. Moreover, the existence of a magnetic field influences the movement of mobile microorganisms in a Hartmann flow. The application of a magnetic field can induce concentrations of the solute within specific regions of the fluid flow. The diffusion rate of the solute is influenced by the Hartmann number, whereby higher Hartmann numbers correspond to reduced diffusion rates. Additionally, the presence of a magnetic field affects the locomotion of motile microorganisms within a Hartmann flow. The presence of a magnetic field has the potential to induce the deflection or capture of microorganisms. The swimming speed of microorganisms is influenced by the Hartmann number, whereby an increase in the Hartmann number results in a decrease in swimming speed. The heat capacity ratio affects the temperature distribution in a Hartmann flow. The temperature distribution exhibits greater uniformity due to the presence of a high heat capacity ratio. The Hartmann number may be used to determine the thickness of the boundary layer when a fluid is flowing through a complicated geometric cavity in the presence of a magnetic field. The magnetic field exerts influence on the adjacent fluid layer, which is a thin layer of fluid in close proximity to the cavity. Fig. 4 depicts the variations of average Nu, Sh, and Nn with respect to γ, considering different values of Ha. It has been observed that the average Nu decreases as the Ha increases. Conversely, the Sh and the Nn exhibit an opposite trend, increasing in value as the Ha increases. The oxygen concentration rate and the swimming speed of microbes in fluid flow are both enhanced by increasing the Ha parameter, which decreases the Lorentz force. A higher Ha indicates a stronger magnetic field, which restricts fluid flow.

4.2. Impact of Rayleigh number (Ra)

Fig. 5 depicts the strong impact of Rayleigh number $Ra = 10^3, 10^4$ and 10^5 on ψ, θ, ξ, N, Cr. The $Ra = \frac{\beta_T g H^3 \Delta T Pr}{\nu^2}$ is a dimensionless parameter that describes the buoyancy-induced convective flow of a fluid. The Rayleigh number is contingent upon the intrinsic characteristics of the fluid, the structural configuration of the enclosure, and the disparity in temperature existing between the enclosing complex shaped enclosures. The flow patterns will initially appear as two distinct vortices, emerging on the left and right sides of the enclosure in a complex geometric enclosure with heated bottom and cooled top walls. As the Rayleigh number exhibits an upward trend, the vortex will undergo a greater degree of elongation, while concurrently witnessing an increase in the complexity of the streamlines. Over time, the vortex will undergo fragmentation, resulting in the formation of multiple vortices that manifest in the uppermost region of the primary vortex. Furthermore, it can be observed that the dimensions of the vertices exhibit a positive correlation with the rise in Ra. As the values of Ra exhibits an upward trend, the isotherms θ within the enclosure undergo a heightened

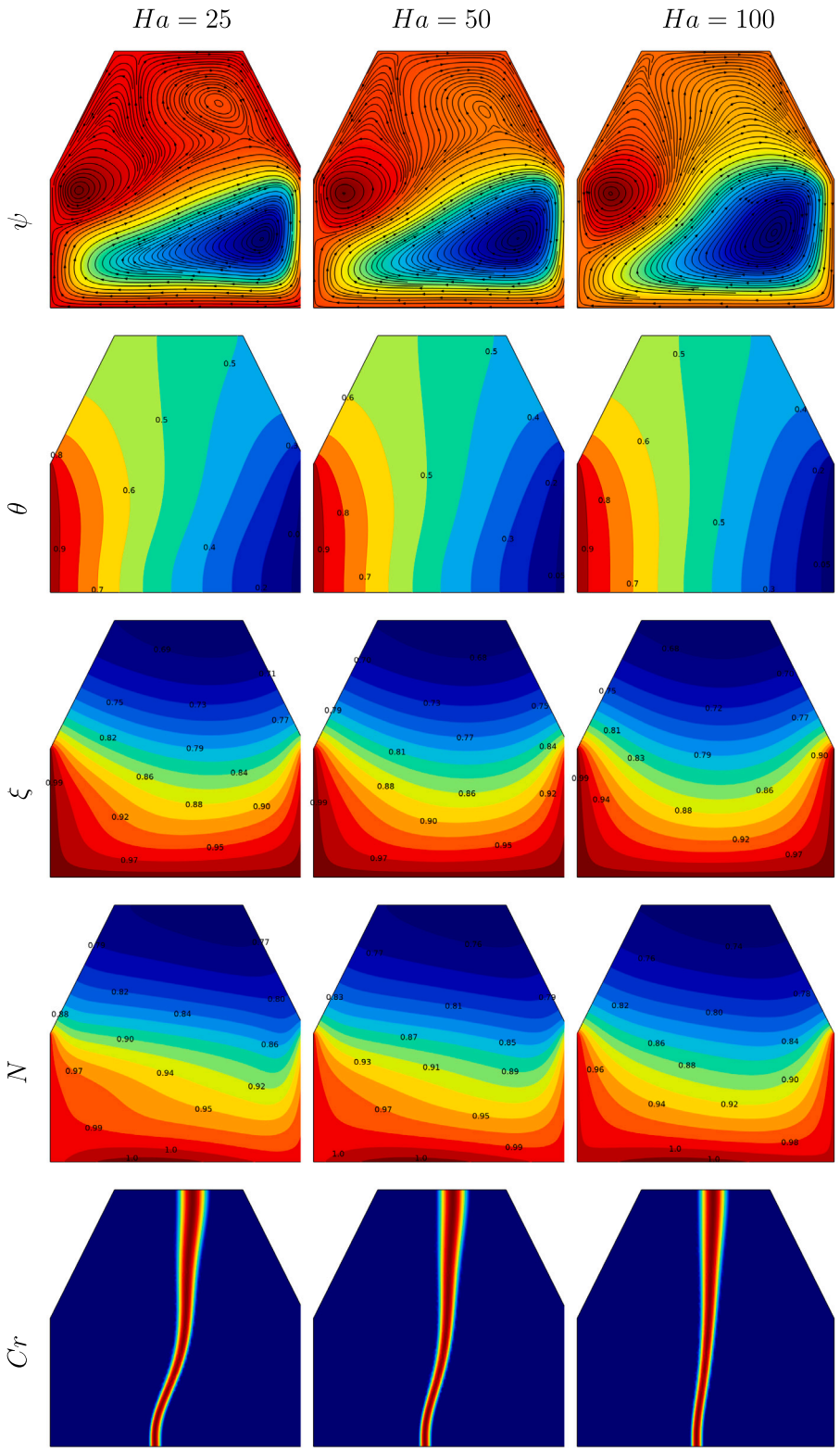

Fig. 3. The contours of ψ, θ, ξ, N, and Cr for the variations of Ha at $Pe = 1, Ste = \theta_f = 0.5, \chi = \zeta = 1, Pr = 6.2, \phi = 0.05, \gamma = 0, Ra = 10^5, Rd = 1,$ and $Rb = 10$.

level of intricacy and distortion in Fig. 5. At low Ra, the isotherms may display a high degree of uniformity or demonstrate relatively uncomplicated patterns. Nevertheless, as the values of Ra increase, the temperature gradients become more prominent, resulting in the emergence of intricate and complex isotherm patterns. The Ra is a crucial parameter that governs the magnitude of convective heat transfer occurring within the enclosed system. An increase in Ra is associated with heightened convective currents, resulting in accelerated rates of heat transfer. The relationship between Ra and oxygen concentration is depicted as a symmetrical, concave upward parabolic curve, which may not always exhibit a linear progression when Ra is incremented. The elevated magnitude of Ra demonstrates the presence of non-uniformity

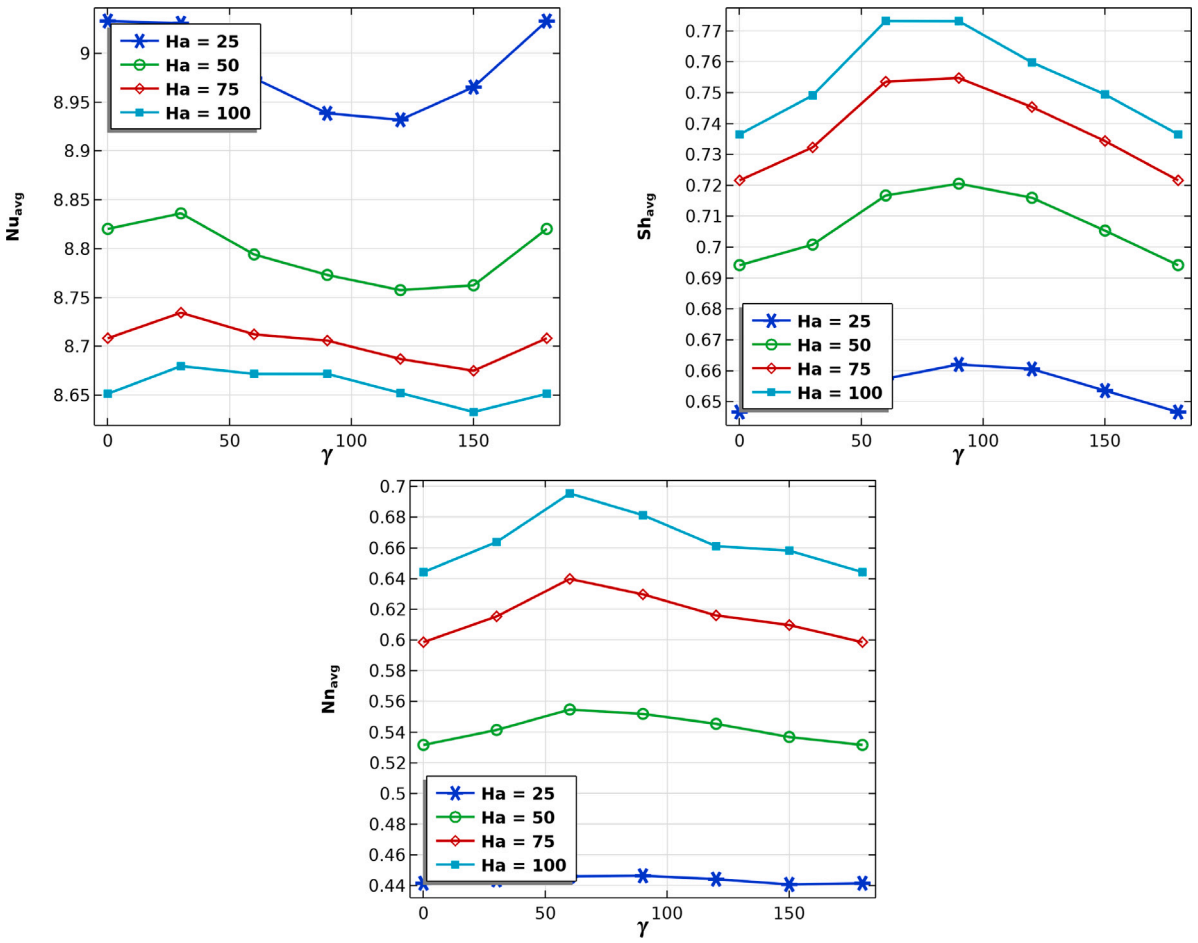

Fig. 4. The Nu_{avg}, Sh_{avg} and Nn_{avg} for the variation of Ha and γ at $Ste = \theta_f = 0.5, \chi = \zeta = 1, Pr = 6.2, \phi = 0.05, Ra = 10^5, Rd = 1,$ and $Rb = 10$.

within the open upward parabolic curve. In certain scenarios, the augmentation of buoyancy-driven convection can result in a reduction in oxygen concentration. This phenomenon occurs due to enhanced convective activity, which can result in the generation of vortices that possess the capability to confine fluid with reduced oxygen content within their central region. The Ra has the potential to influence the behavior and spatial arrangement of motile microorganisms, as depicted in Fig. 5. Convective motion may occur within the enclosure when the Ra surpasses a specific critical threshold. The process of convection has the potential to facilitate the homogenization of nutrients, chemicals, and oxygen, thereby exerting an impact on the spatial arrangement of mobile microorganisms. Regions characterized by higher Ra can potentially exhibit more intense convection and increased mixing, which can have implications for the availability of resources for motile microorganisms. The formation of vortices in a complex enclosure shape can be influenced by the Ra. As the Ra exhibits an upward trend, the vortices become more discernible, thereby potentially resulting in heightened fluid mixing. The influence of the Ra on the heat capacity ratio within a complex-shaped enclosure is contingent upon the precise characteristics of the enclosure's geometry. In a broader context, it can be observed that the Ra serves as an indicator of the magnitude of the buoyancy forces responsible for propelling natural convection. As the Ra escalates, the buoyancy forces experience amplification, leading to a typical reduction in the heat capacity ratio. The enhanced fluid mixing resulting from buoyancy forces leads to a reduction in temperature gradients and heat capacity ratios. The graph exhibits a distinct division into two symmetrical and homogeneous sections when $Ra = 10^3$. If the $Ra(= 10^4, 10^5)$ increases, there is a possibility for the transformation of uniform regions into non-uniform regions, resulting in a conversion of the core component's motion from linear to nonlinear. Fig. 6 shows the average $Nu, Sh,$ and Nn as a function of the Rb and Ra. The figure demonstrates a notable observation wherein, for higher Rb, a sudden increase is observed across all plots, including the $Nu, Sh,$ and Nn. In the scenario where the Ra is not considered, there is an observed increase in the Nu. Conversely, when the Ra is taken into account, a decrease in the Nu is observed. The observed behavior of both Sh, and Nn exhibits a mixed pattern as the values of the Rb and Ra increase.

4.3. Impact of thermal radiation (Rd)

Fig. 7 illustrates the significant influence of thermal radiation ($Rd = 0, 2, 4$) on ψ, θ, ξ, N, Cr. The occurrence of the tri-vortex phenomenon in the streamlines is observed when the thermal radiation Rd approaches zero. The intensity of the bolus vortex is positively correlated with higher levels of thermal radiation. In the case of a complex enclosure with a uniform temperature, it can be observed that for higher values of thermal radiation, the isotherm lines within the enclosure would exhibit a linear pattern. Nevertheless, within a geometrically intricate enclosure where thermal radiation is absent, the isotherms may exhibit curvature or irregularity. Isotherm distortion is directly proportional to both the amount of heat radiation and the complexity of the enclosure. In cases when concentration occurs near the heated enclosure wall, which has a complicated form, the number of contours has been increased due to the intensified values of the thermal radiation parameter. A comparable pattern can be observed in the distribution of motile microorganisms. The influence of Rd on the heat capacity ratio can be observed in Fig. 7, presented in a contour format. In the absence of thermal radiation, the contour graph depicting the heat

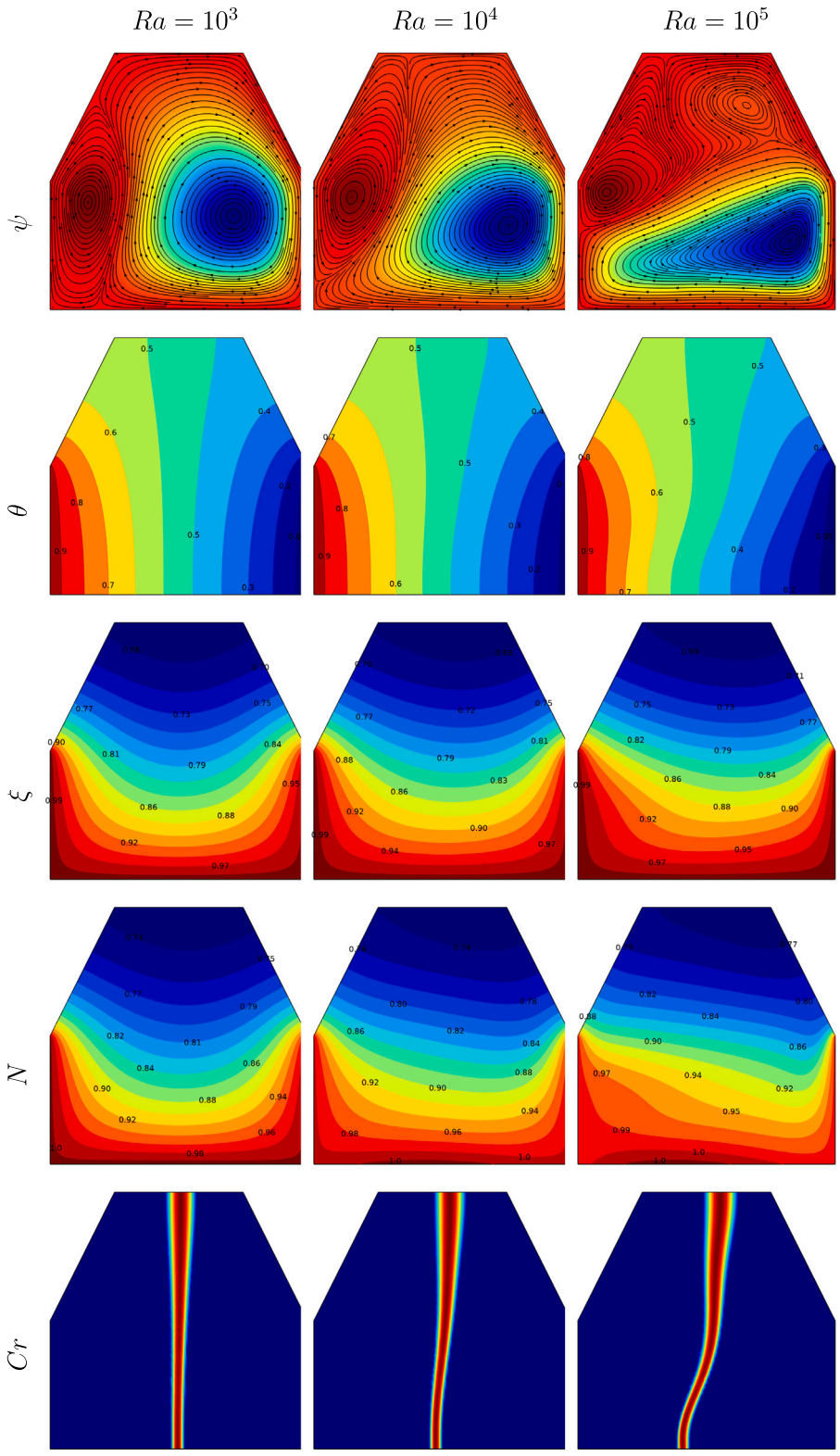

Fig. 5. The contours of ψ, θ, ξ, N, and Cr below the variations of Ra at $Pe = 1, Ste = \theta_f = 0.5, \chi = \zeta = 1, Pr = 6.2, \phi = 0.05, Ha = 25, \gamma = 0, Rd = 1,$ and $Rb = 10$.

capacity ratio exhibits a nonlinear pattern characterized by streamlines. The heat capacity ratio exhibits a linear pattern in response to higher values of thermal radiation, indicating the influence of the complex shape of enclosures. Fig. 8 shows the Nu, Sh, and Nn as a function of the Rd and E. The Nusselt number exhibits a consistent and linear growth pattern as the thermal radiation parameter increases, while keeping the activation energy constant. Because radiation warms the material in question directly, temperature gradients close to the heat source become more pronounced. As a result, the total heat transfer rate is increased since conduction and convection are both driven more strongly. The inclusion of thermal radiation as a supplementary heat transfer mechanism can effectively augment the overall rate of heat

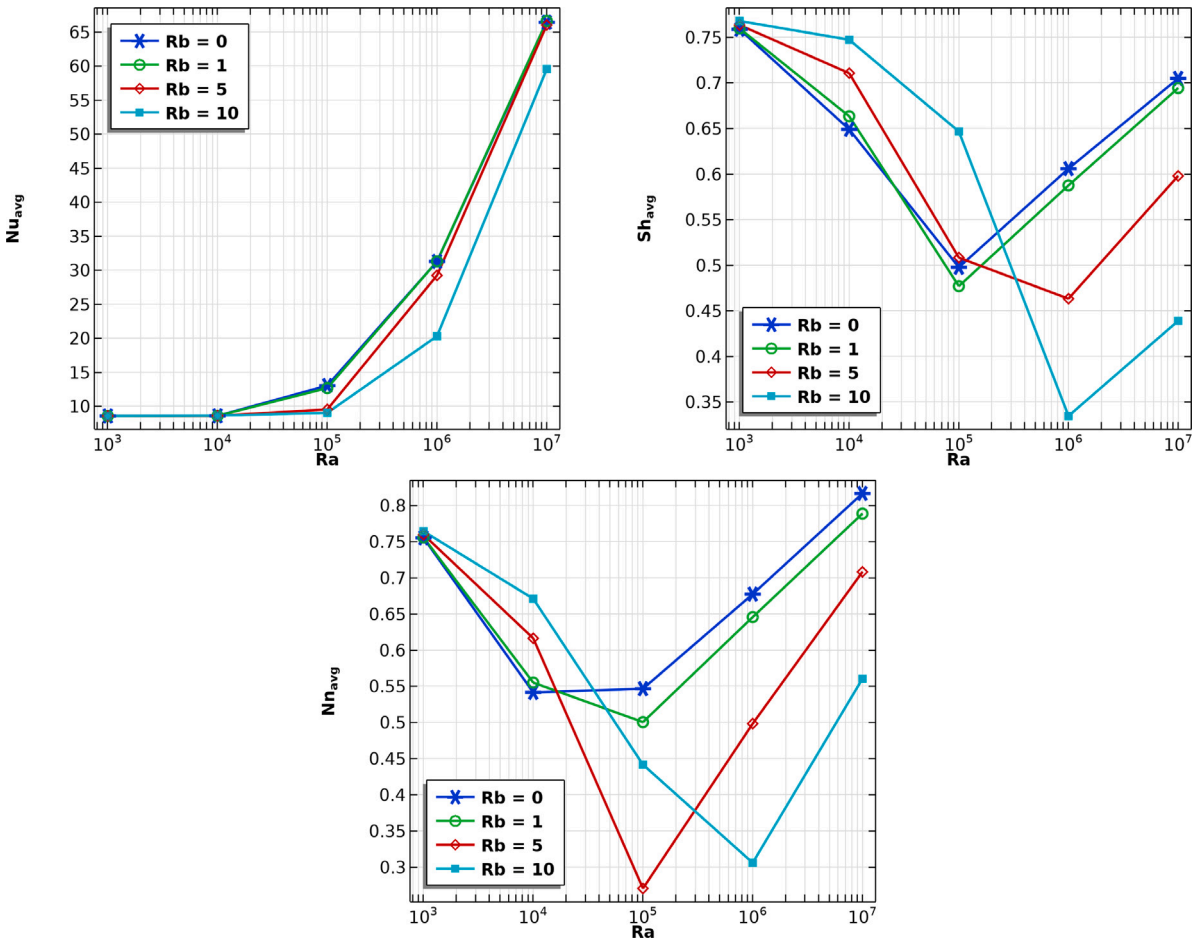

Fig. 6. The Nu_{avg}, Sh_{avg} and Nn_{avg} for the variation of Rb and Ra at $Ste = \theta_f = 0.5, \chi = \zeta = 1, Pr = 6.2, \phi = 0.05, Ha = 25, \gamma = 0, Rd = 1$.

transfer. The analysis suggests that the mean velocity of swimming and population density of mobile microorganisms exhibit a positive correlation with both the Rd and E (see Fig. 3).

4.4. Impact of Lewis number (Le)

Fig. 9 illustrates the significant influence of the Lewis number Le values of $0.1, 1$, and 10 on the variables ψ, θ, ξ, N, Cr. The presence of two vortex centers in close proximity to the complex shaped walls is noted for lower values of the Lewis number. However, as the Lewis number approaches unity, the top vortex centers vanish and transform into two micro-bolus structures. Vortex centers have been observed for higher Lewis number. Additionally, the streamlines become more pronounced as the Lewis number increases. It has been discovered that thermal energy is able to permeate throughout the enclosure, with the exception of the higher walls. This phenomenon leads to temperatures that are mostly increased in the vicinity of the lower walls of the nanofluid. Subsequently, as a consequence of elevated temperatures experienced by the lower wall of a structurally intricate enclosure, discernible alterations in the isotherm patterns occur. For a given concentration near the bottom wall of a heated enclosure, the number of contours has increased as the Lewis number has increased. The distribution of motile microorganisms follows a similar pattern, with the vortex centers being detected at the middle of the complex walls. When the Lewis number is low, the rate of mass diffusion is expected to be slower compared to the rate of heat conduction. The consequence of this phenomenon is the emergence of a non-homogeneous temperature distribution within the enclosure, wherein the temperature in close proximity to the center of the intricately shaped wall exhibits a significantly higher value compared to the temperature of the heated fluid. This phenomenon will result in an elevation of the heat capacity ratio, as the enclosure will exhibit an enhanced capacity to retain and accumulate thermal energy. The impact of Le and Pe on the Nu, Sh, and Nn have been portrayed in Fig. 10. The figure illustrates a noticeable decline in all plots, including average Nu and Sh, for higher values of Pe. The minimal value of the Pe is associated with a higher average Nu. This revised behavior is observed in the average Sh and Nn. The average Sh exhibits mixed behavior as the values of Le and Pe increase. The analysis illustrates a positive correlation between the average Nn and the variables Le and Pe. This combination favors fast transfer of both Nu, Sh, and Nn. Rapid diffusion aided by strong convection leads to efficient removal of energy, species, motile microorganisms and from the surface.

5. Conclusions

The present study focuses on the computational analysis of the MHD bioconvection flow of NEPCMs within a complexly shaped enclosure. The effects of factors such as thermal radiation, activation energy and oxytactic microorganisms have also been taken into account. The flow model is calculated using the sophisticated finite element method. The present study illustrates the effects of various parameters on the characteristics of the ψ, θ, ξ, N, Cr, average Nu, Sh and Nn profiles using visual representations. The primary outcomes of the present study are as follows:

- Increases in the Ha and the Le reduce the number of bolus in contour streamlines, whereas increases in the Rd have been shown to increase the number of bolus in streamlines.

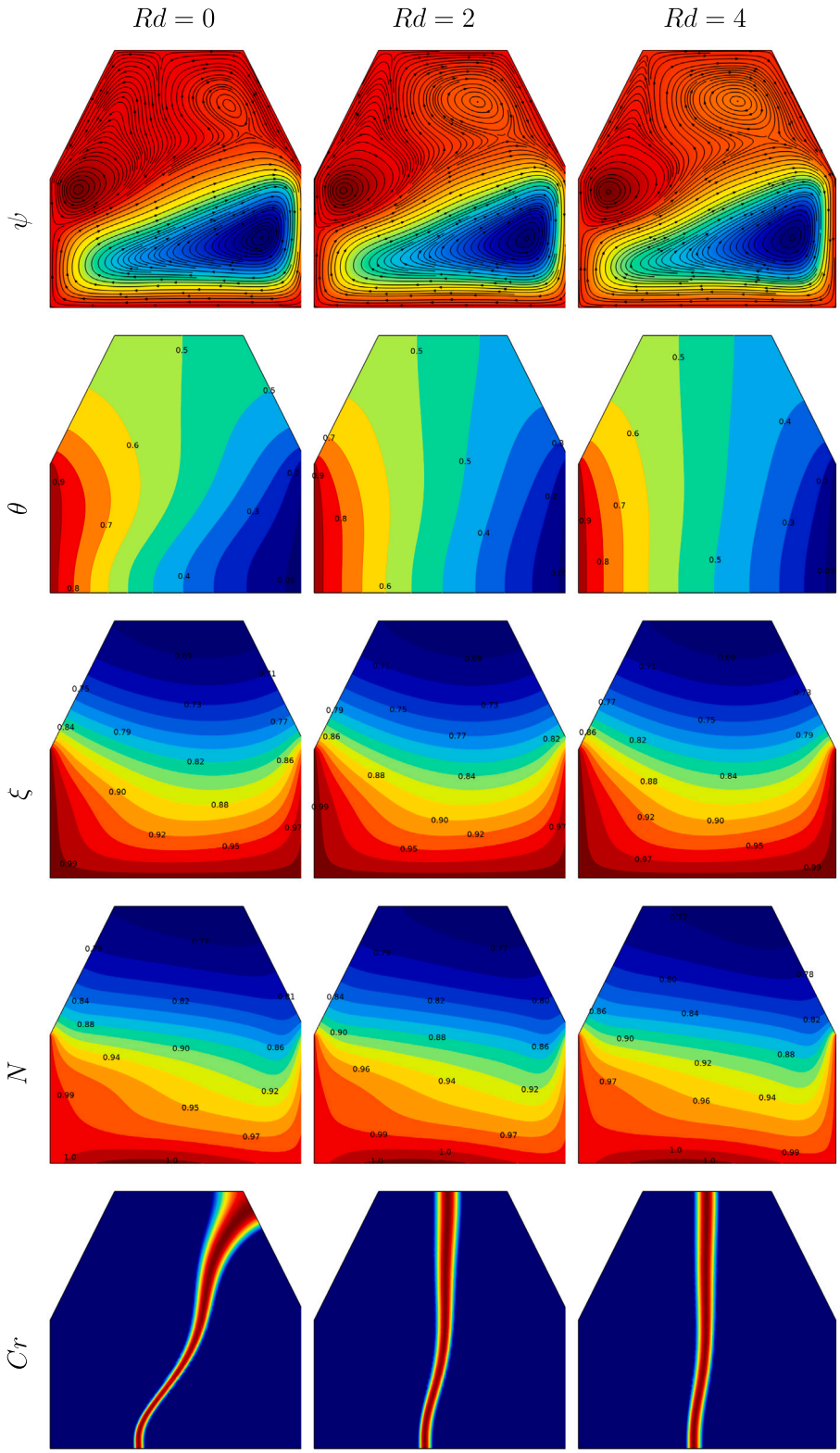

Fig. 7. The contours of ψ, θ, ξ, N, and Cr for the variations of Rd at $Pe = 1, Ste = \theta_f = 0.5, \chi = \zeta = 1, Pr = 6.2, \phi = 0.05, Ha = 25, \gamma = 0, Ra = 10^5$, and $Rb = 10$.

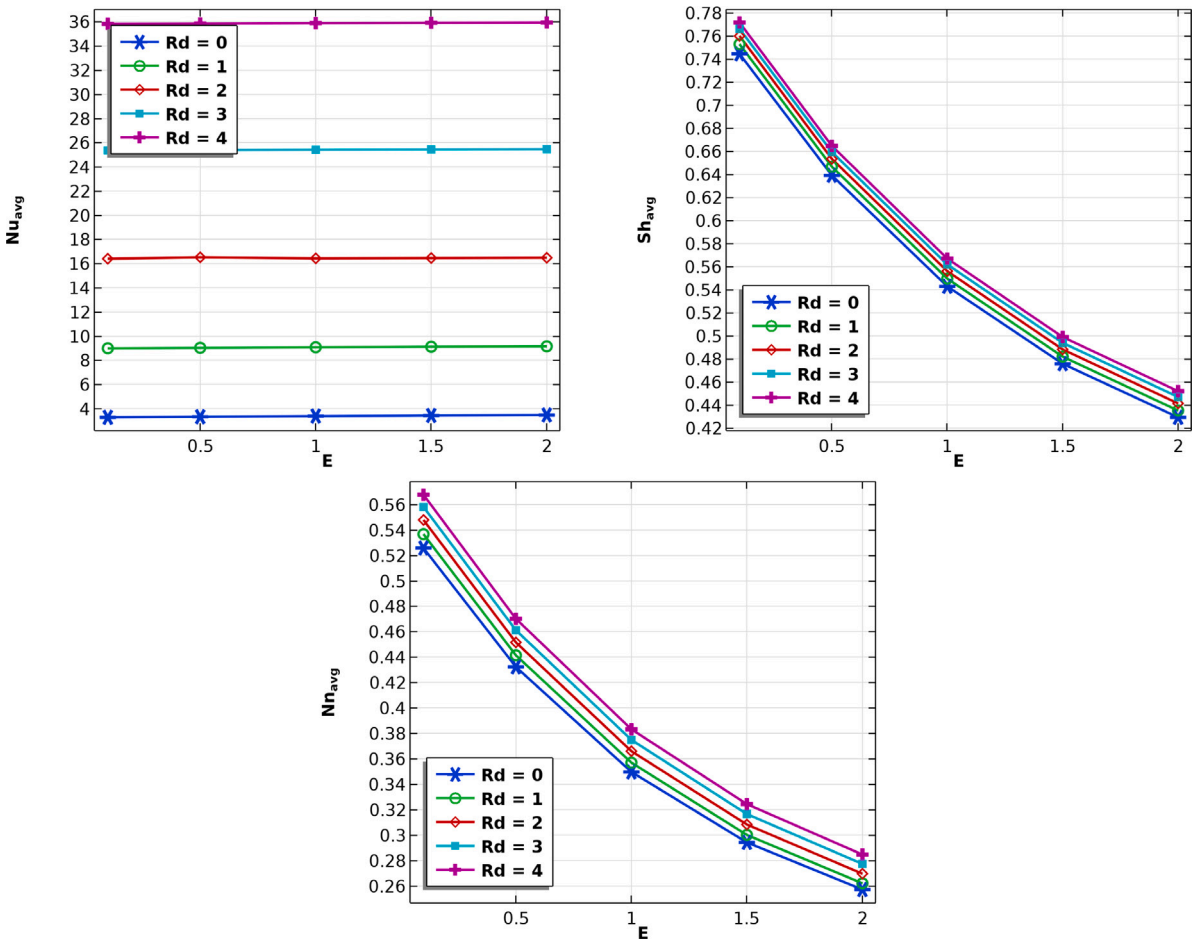

Fig. 8. The Nu_{avg}, Sh_{avg} and Nn_{avg} for the variation of Rd and E at $Ste = \theta_f = 0.5, \chi = \zeta = 1, Pr = 6.2, \phi = 0.05, Ha = 25, \gamma = 0, Ra = 10^5$, and $Rb = 10$.

- Rd and Ha have a significant impact on heat transmission. Increased Rd enhances heat transfer. The heat transfer rate falls as Ha rises because convective fluxes weaken.
- Increasing magnetic field intensity decreases convection heat transfer, reducing cavity re-circulation eddy. After that, conduction heat transfer dominates.
- The Nu exhibits a decreasing trend as the Ha, Rb and Pe increases.
- The Sh and Nn exhibit a positive correlation with the Ha and Rd.
- For greater values of Le in the oxygen concentration contour graph, the vortex centers have been formed towards the bottom walls.
- In the oxygen concentration and motile microorganisms contour graphs, it can be observed that as the Le value increases, the vortex centers tend to form closer to the bottom walls.

The future work of this research on NEPCMs could involve several avenues for exploration and refinement. Firstly, there is an opportunity to extend the investigation to include a wider range of nanoparticle concentrations and types, exploring their effects on bioconvection flow within the rectotrapezoidal cavity. Additionally, further analysis could be conducted on the interaction between multiple parameters, such as the simultaneous influence of inclined magnetic fields, oxytactic bacteria, radiation, and Lewis number on the bioconvection flow of NEPCMs. The study could also benefit from exploring different cavity geometries and boundary conditions to assess the robustness and generalizability of the findings.

CRediT authorship contribution statement

Shafqat Hussain: Writing – review & editing, Visualization, Validation, Software, Methodology, Investigation, Formal analysis, Data curation, Conceptualization. **Prakash Jayavel:** Writing – review & editing, Writing – original draft, Conceptualization. **Bander Almutairi:** Writing – original draft, Visualization, Investigation, Formal analysis, Conceptualization. **Katta Ramesh:** Writing – review & editing, Writing – original draft, Conceptualization.

Declaration of competing interest

The authors declare that they have no known competing financial interests or personal relationships that could have appeared to influence the work reported in this paper.

Data availability

Data will be made available on request.

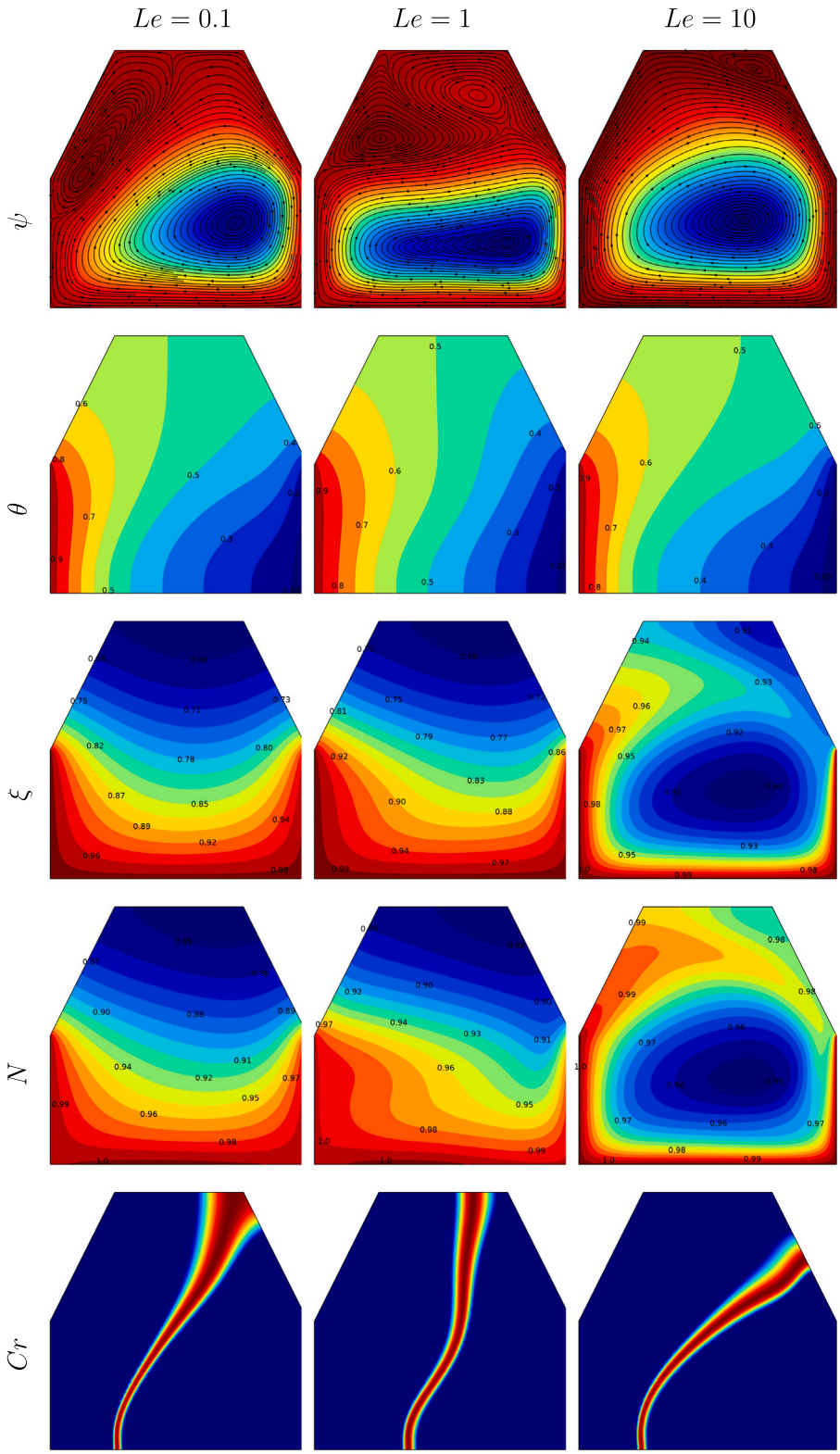

Fig. 9. The contours of ψ, θ, ξ, N, and Cr for the variations of Le at $Pe = 0.5, Ste = \theta_f = 0.5, \chi = \zeta = 1, Pr = 6.2, \phi = 0.05, Ha = 25, \gamma = 0, Ra = 10^5$, and $Rb = 10$.

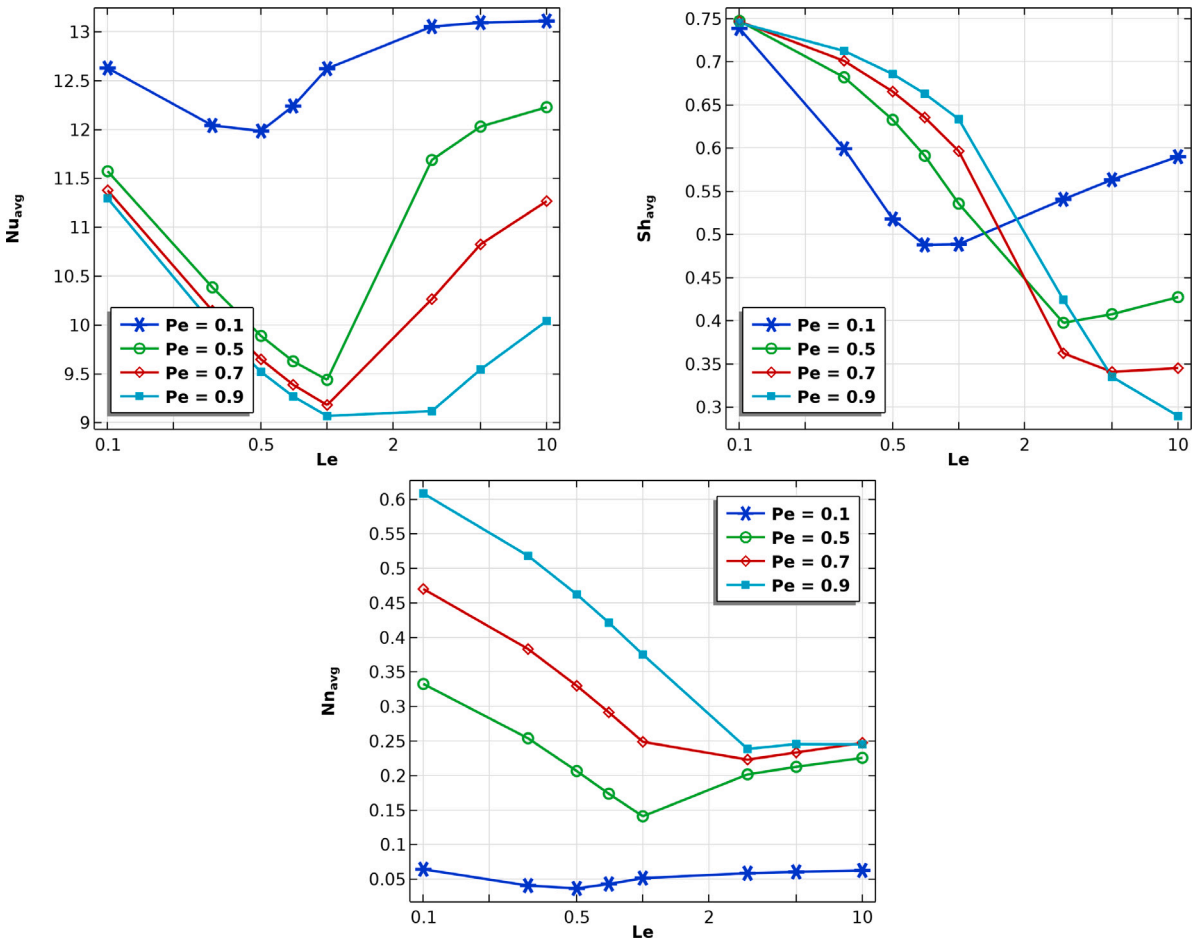

Fig. 10. The Nu_{avg}, Sh_{avg} and Nn_{avg} for the variation of Pe and Le at $Ste = \theta_f = 0.5, \chi = \zeta = 1, Pr = 6.2, \phi = 0.05, Ha = 25, \gamma = 0, Ra = 10^5$, and $Rb = 10$.

Acknowledgments

Third author is supported by Researchers Supporting Project number: RSPD2024R650, King Saud University, Saudi Arabia, Riyadh, Saudi Arabia.

References

[1] J.M. Khodadadi, S.F. Hosseinizadeh, Nanoparticle-enhanced phase change materials (NEPCMs) with great potential for improved thermal energy storage, Int. Commun. Heat Mass Transfer 34 (5) (2007) 534–543.

[2] S. Shaikh, K. Lafdi, K. Hallinan, Carbon nanoadditives to enhance latent energy storage of phase change materials, J. Appl. Phys. 103 (9) (2008).

[3] Y. El Hasadi, J.M. Khodadadi, Numerical simulation of solidification of nanoparticle-enhanced phase change materials (NEPCMs) considering transport of suspensions, in: TMNN-2010. Proceedings of the International Symposium on Thermal and Materials Nanoscience and Nanotechnology, Begel House Inc, 2011.

[4] P. Murugan, P.Ganesh. Kumar, V. Kumaresan, M. Meikandan, K.Malar. Mohan, R. Velraj, Thermal energy storage behaviour of nanoparticle enhanced PCM during freezing and melting, Phase Transit. 91 (3) (2018) 254–270.

[5] M.A.M. Irwan, C.N. Azwadi, Y. Asako, J. Ghaderian, Review on numerical simulations for nano-enhanced phase change material (NEPCMs) phase change process, J. Therm. Anal. Calorim. 141 (2020) 669–684.

[6] R. Li, Y. Zhou, X. Duan, Nanoparticle enhanced paraffin and tailing ceramic composite phase change material for thermal energy storage, Sustain. Energy Fuels 4 (9) (2020) 4547–4557.

[7] J.I. Prado, L. Lugo, Enhancing the thermal performance of a stearate phase change material with graphene nanoplatelets and MgO nanoparticles, ACS Appl. Mater. Interfaces 12 (35) (2020) 39108–39117.

[8] S.L. Tariq, H.M. Ali, M.A. Akram, M.M. Janjua, M. Ahmadlouydarab, Nanoparticles enhanced phase change materials (NEPCMs)-A recent review, Appl. Therm. Eng. 176 (2020) 115305.

[9] H. Faraji, M.E. Alami, A. Arshad, Y. Hariti, Numerical survey on performance of hybrid NEPCMs for cooling of electronics: Effect of heat source position and heat sink inclination, J. Therm. Sci. Eng. Appl. 13 (5) (2021) 051010.

[10] M. Jafarian, M. Delgado, M. Omid, M. Khanali, M. Mokhtari, A. Lázaro, Enhancing thermophysical properties of phase change material via alumina and copper nanoparticles, Int. J. Energy Res. 46 (5) (2022) 6594–6612.

[11] M.A. Amidu, M. Ali, A.K. Alkaabi, Y. Addad, A critical assessment of nanoparticles enhanced phase change materials (NEPCMs) for latent heat energy storage applications, Sci. Rep. 13 (1) (2023) 7829.

[12] A.A.R. Darzi, M. Farhadi, M. Jourabian, Y. Vazifeshenas, Natural convection melting of NEPCMs in a cavity with an obstacle using lattice Boltzmann method, Internat. J. Numer. Methods Heat Fluid Flow 24 (1) (2014) 221–236.

[13] R. Elbahjaoui, H. El Qarnia, M. El Ganaoui, Melting of nanoparticle-enhanced phase change material inside an enclosure heated by laminar heat transfer fluid flow, Eur. Phys. J. Appl. Phys. 74 (2) (2016) 24616.

[14] R. Elbahjaoui, H. El Qarnia, Melting of nanoparticle-enhanced phase change material in a shell-and-tube latent heat storage unit heated by laminar pulsating fluid flow, Comput. Therm. Sci. 9 (4) (2017).

[15] M. Ghalambaz, A. Doostani, A.J. Chamkha, M.A. Ismael, Melting of nanoparticles-enhanced phase-change materials in an enclosure: effect of hybrid nanoparticles, Int. J. Mech. Sci. 134 (2017) 85–97.

[16] H. Masoumi, R. Haghighi Khoshkhoo, Investigation of melting of nanoparticle-enhanced phase change materials (NEPCMs) in a shell-and-tube heat exchanger with longitudinal fins, Heat Mass Transf. 57 (2021) 681–701.

[17] M. Ghalambaz, S.A.M. Mehryan, A. Hajjar, M.Y.A. Shdaifat, O. Younis, P. Talebizadehsardari, W. Yaïci, Thermal charging optimization of a wavy-shaped nano-enhanced thermal storage unit, Molecules 26 (5) (2021) 1496.

[18] A. Abderrahmane, M. Al-Khaleel, A. Mourad, H. Laidoudi, Z. Driss, O. Younis, et al., Natural convection within inversed T-shaped enclosure filled by nano-enhanced phase change material: Numerical investigation, Nanomaterials 12 (17) (2022) 2917.

[19] S. Hussain, A.M. Aly, N. Alsedias, Bioconvection of oxytactic microorganisms with nano-encapsulated phase change materials in an omega-shaped porous enclosure, J. Energy Storage 56 (2022) 105872.

[20] S. Hussain, F. Ertam, M.B.B. Hamida, H.F. Oztop, N.H. Abu-Hamdeh, Analysis of bioconvection and oxytactic microorganisms in a porous cavity with nano-enhanced phase change materials and quadrant heater: Application of support vector regression based model, J. Energy Storage 63 (2023) 107059.
[21] R. Qahiti, A. Almarashi, W. Hamali, Thermal behavior of nanoparticle enhanced phase change material discharging in existence of complex geometry, J. Energy Storage 59 (2023) 106450.
[22] M. Abdi, K. Chaib, A. Menouer, S. Benferhat, A natural convection conjugate heat transfer of nano-encapsulated phase change materials (NEPCMs) in an inclined blocked square enclosure, Numer. Heat Transfer A 84 (6) (2023) 604–625.
[23] A. Rahmani, M. Dibaj, M. Akrami, Computational investigation of magnetohydrodynamic flow and melting process of phase change material in a battery pack using the lattice Boltzmann method, J. Energy Storage 78 (2024) 110046.
[24] A.M. Aly, Z. Raizah, S. El-Sapa, H.F. Oztop, N. Abu-Hamdeh, Thermal diffusion upon magnetic field convection of nano-enhanced phase change materials in a permeable wavy cavity with crescent-shaped partitions, Case Stud. Therm. Eng. 31 (2022) 101855.
[25] O. Younis, A. Abderrahmane, M. Hatami, A. Mourad, K. Guedri, Nanoencapsulated phase change material in a trapezoidal prism wall under the magnetic field effect for energy storage purposes, Sci. Rep. 13 (1) (2023) 16060.
[26] M. Zandie, A. Moghaddas, A. Kazemi, M. Ahmadi, H.N. Feshkache, M.H. Ahmadi, M. Sharifpur, The impact of employing a magnetic field as well as Fe3O4 nanoparticles on the performance of phase change materials, Eng. Appl. Comput. Fluid Mech. 16 (1) (2022) 196–214.
[27] S.M.H. Zadeh, S.A.M. Mehryan, M.S. Islam, M. Ghalambaz, Irreversibility analysis of thermally driven flow of a water-based suspension with dispersed nano-sized capsules of phase change material, Int. J. Heat Mass Transfer 155 (2020) 119796.
[28] S. Hussain, M. Molana, T. Armaghani, A.M. Rashad, H.A. Nabwey, Energy storage performance and irreversibility analysis of a water-based suspension containing nano-encapsulated phase change materials in a porous staggered cavity, J. Energy Storage 53 (2022) 104975.
[29] A. Alazzam, N.A.A. Qasem, A. Aissa, M.S. Abid, K. Guedri, O. Younis, Natural convection characteristics of nano-encapsulated phase change materials in a rectangular wavy enclosure with heating element and under an external magnetic field, J. Energy Storage 57 (2023) 106213.
[30] S. Hussain, Z. Raizah, A.M. Aly, Thermal radiation impact on bioconvection flow of nano-enhanced phase change materials and oxytactic microorganisms inside a vertical wavy porous cavity, Int. Commun. Heat Mass Transfer 139 (2022) 106454.
[31] S. Hussain, F. Schieweck, S. Turek, Efficient Newton-multigrid solution techniques for higher order space–time Galerkin discretizations of incompressible flow, Appl. Numer. Math. 83 (2014) 51–71, http://dx.doi.org/10.1016/j.apnum.2014.04.011.
[32] S. Hussain, K. Mehmood, M. Sagheer, A. Farooq, Entropy generation analysis of mixed convective flow in an inclined channel with cavity with Al2O3-water nanofluid in porous medium, Int. Commun. Heat Mass Transf. 89 (2017) 198–210, http://dx.doi.org/10.1016/j.icheatmasstransfer.2017.10.009.
[33] S. Hussain, S. Shoeibi, T. Armaghani, Impact of magnetic field and entropy generation of casson fluid on double diffusive natural convection in staggered cavity, Int. Commun. Heat Mass Transf. 127 (2021) 105520, http://dx.doi.org/10.1016/j.icheatmasstransfer.2021.105520.
[34] B. Ghasemi, S.M. Aminossadati, A. Raisi, Magnetic field effect on natural convection in a nanofluid-filled square enclosure, Int. J. Therm. Sci. 50 (2011) 1748–1756, http://dx.doi.org/10.1016/j.ijthermalsci.2011.04.010.